Characterization of ferroelectric hafnium/zirconium oxide solid solutions deposited by reactive magnetron sputtering

Jordan Bouaziz, Pedro Rojo Romeo, Nicolas Baboux, Bertrand Vilquin

Characterization of ferroelectric hafnium/zirconium oxide solid solutions deposited by reactive magnetron sputtering

Jordan Bouaziz, Pedro Rojo Romeo, Nicolas Baboux, and Bertrand Vilquin

Citation: Journal of Vacuum Science & Technology B **37**, 021203 (2019); doi: 10.1116/1.5060643
View online: https://doi.org/10.1116/1.5060643
View Table of Contents: https://avs.scitation.org/toc/jvb/37/2
Published by the American Vacuum Society

Characterization of ferroelectric hafnium/zirconium oxide solid solutions deposited by reactive magnetron sputtering

Jordan Bouaziz,[1,2,a] Pedro Rojo Romeo,[1,b] Nicolas Baboux,[2,c] and Bertrand Vilquin[1,d]
[1]*Université de Lyon, Institut des Nanotechnologies de Lyon (UMR5270/CNRS), Ecole Centrale de Lyon, 36 avenue Guy de Collongue, F-69134 Ecully Cedex, France*
[2]*Université de Lyon, Institut des Nanotechnologies de Lyon (UMR5270/CNRS), INSA, Bât. Blaise Pascal, 7 avenue Jean Capelle, F-69621 Villeurbanne Cedex, France*

(Received 21 September 2018; accepted 14 January 2019; published 6 February 2019)

The room temperature deposition of 10 nm-thick ferroelectric hafnium/zirconium oxide, (Hf, Zr)O_2, thin solid films is achieved with a single hafnium/zirconium, Hf/Zr, alloy target by reactive magnetron sputtering. After rapid thermal annealing (RTA), crystallization of our samples is analyzed by grazing incidence x-ray diffraction. Changing the pressure inside the chamber during deposition leads to grow amorphous or monoclinic phase (m-phase). The authors demonstrate that if the (Hf, Zr)O_2 films are crystallized in the m-phase after deposition, no ferroelectric/orthorhombic phase can be obtained further. On the contrary, when the as-deposited film is amorphous, the ferroelectric/orthorhombic phase appears after the RTA. *Published by the AVS.* https://doi.org/10.1116/1.5060643

I. INTRODUCTION

Among several ferroelectric HfO_2 applications the most addressed are negative-capacitance field effect transistor (NC-FET)[1,2] and ferroelectric random access memory (FRAM).[3,4] They have in common the use of a capacitor whose insulator is the ferroelectric HfO_2. For the time being, the stabilization of the ferroelectric phase in (un)doped HfO_2 on silicon faces some issues. It results in difficulties to build a metal/ferroelectric/semiconductor (MFS) architecture, delaying further transistor applications using MFS interface. On the contrary, FRAM in the $1T-1C$ architecture allows one to grow ferroelectric HfO_2 on appropriate materials such as titanium nitride, for instance. Consequently, FRAM in the $1T-1C$ architecture has never seemed so close to massive industrialization.

Internet of things sensor node requires to process data at the source. These systems need highly energy efficient microprocessor units (MCUs) using embedded nonvolatile memories (eNVM). MCU often uses a combination of flash and RAM memories. However, flash technology suffers from a limited endurance, low write speed, and scalability issues. They need high voltage during the writing step, which implies the use of charge pumps. An alternative fast, low power, and high endurance eNVM could greatly enhance energy efficiency.

At the beginning, FRAM was built with ferroelectric perovskite insulators. However, perovskites show scalability issues,[5,6] while ferroelectric HfO_2 has never stopped being improved to fit with industrial requirements since its discovery in 2011.[7] At the present time, it appears as a promising candidate to realize new efficient FRAM: HfO_2 processes are already integrated in the Si CMOS industry, and their ferroelectric properties are adequate for using oxide layer thinner than 10 nm.[8] Nevertheless, some of its properties could still be greatly improved for industrial applications.

As a consequence, the nucleation and stabilization of the ferroelectric phase (f-phase) has to be fully understood; the f-phase is attributed to the polar orthorhombic phase corresponding to the $Pca2_1$ space group (f-phase),[9] but other phases are generally present inside the oxide after the growth, due to stabilization issues.

Many dopants have been used since 2011: Si (Ref. 7), Y (Ref. 10), Zr (Ref. 11), Al (Ref. 12), Gd (Ref. 13), Sr (Ref. 14), La (Ref. 15), Sm (Ref. 16), Yb, Nd, Er (Ref. 17), Mg, Ba, Co, Ni, Ga, In (Ref. 18), and N (Ref. 19). However, further studies need to be done to obtain all the requirements fitting with industry and the possibility of using many dopants adds a difficulty in the complete understanding of the nucleation and the stabilization of the f-phase.

The dopant on which most investigations have been done is clearly Zr^{4+}. It is because its annealing temperature seems to be the lowest of all dopants (or undoped HfO_2) and both HfO_2 and ZrO_2 are already used for DRAM mass production. This is the reason why we will focus on Zr doping in this paper.

The presence of the f-phase in (Hf, Zr)O_2 solid solution has mostly been studied by atomic layer deposition (ALD)[2,7,8,11,20–42] and metal organic chemical vapor deposition (MOCVD),[43–47] but some papers have also studied (Hf, Zr)O_2 solid solution by chemical solution deposition (CSD),[48,49] pulsed laser deposition (PLD),[50] cosputtering,[51–54] or sputtering with a single HfO_2/ZrO_2 target.[55–58] Nonetheless, the electrodes are often deposited by physical vapor deposition (PVD) because it could enhance ferroelectricity, at least if the top electrode is deposited by PVD.[59] Above all, compared to ALD deposition, sputtering is extremely faster (cf. deposition speeds in Table I). Furthermore, it is hard to separate Hf and Zr. Therefore, industrial processes are usually expensive. For instance, when an industrial manufacturer gives the impurities in an Hf or HfO_2 sputtering target, it does not include Zr impurities. It could be interesting to have only one process where

Note: This paper is part of the Conference Collection from the 20th Workshop on Dielectrics in Microelectronics Conference.
[a]Electronic mail: jordan.bouaziz@insa-lyon.fr
[b]Electronic mail: pedro.rojo-romeo@ec-lyon.fr
[c]Electronic mail: nicolas.baboux@insa-lyon.fr
[d]Electronic mail: bertrand.vilquin@ec-lyon.fr

TABLE I. Deposition details and film growth conditions.

Sputtering deposition details		
Target size	101.0 mm (≈ 4 in.) diameter, 3 mm thickness	
Target–substrate distance	8 cm	
Substrate temperature	Room temperature	
Base pressure	$< 5 \times 10^{-7}$ mbar	
Ignition pressure	5×10^{-2} mbar	
Deposited elements	TiN	(Hf, Zr)O_2
Target	Ti (99.995%)	Hf/Zr (99.9%)
Substrate	Si(100)	Si(100)/TiN
Working pressure	5×10^{-3} mbar	5×10^{-3} mbar or 5×10^{-2} mbar
Target RF power	300 W	100 W
Holder DC bias voltage	60 V	None
Gas	Ar = 50 sccm; N_2 = 3 sccm	Ar = 50 sccm; O_2 = 10 sccm
Deposition speed	5.0 nm/min	≈ 0.83 nm/min
Rapid thermal annealing (RTA) conditions		
Temperature variation	400/500/600 °C	
Atmosphere	N_2	
Time	30 s	

the separation of Hf and Zr is not needed. Also, using a single target like Hf/Zr or HfO_2/ZrO_2 could ease cosputtering like, for example, the realization of 1% La-doped $Hf_{0.5}Zr_{0.5}O_2$ as it shows a low annealing temperature and a very promising endurance and remnant polarization.[28] Finally, ALD is a chemical deposition process, whereas sputtering is a physical deposition process. To fully understand the ferroelectricity in HfO_2, it seems crucial to compare and understand common features and differences such as energies of the incident atoms during deposition, stress and strain relations, and the appearance or absence of crystalline phases of interest according to the different deposition conditions, observing differences in the electrical characterizations because of the presence of an oxide interfacial layer for instance, etc.

In addition, if some papers show results for a single HfO_2/ZrO_2 target[55–58] in sputtering, to our knowledge, using a single Hf/Zr target has never been tried, while sputtering from a metallic target generally needs low sputtering power and it could be difficult to transfer high powers in industrial facilities. Also, with the same amount of dioxygen, sputtering deposition is supposed to be faster with a metallic target than with a ceramic one.

Consequently, in this article, we will focus on the deposition of 10 nm-thick (Hf, Zr)O_2 solid solutions by reactive magnetron sputtering from a single Hf/Zr alloy target between two titanium nitride electrodes and compare our first results with other techniques.

II. EXPERIMENTAL DETAILS

A. Fabrication

Before deposition, Si(100) oriented substrate is cleaned in acetone and ethanol, then the native oxide layer is removed by the buffered oxide etch (BOE) process. All depositions are done by magnetron sputtering at room temperature in the same sputtering equipment: an AC-450 sputtering machine by Alliance Concept. TiN thin films are deposited onto the substrate by radio frequency (RF) reactive magnetron sputtering system using a high purity titanium target in a mixture of argon and nitrogen gas. We deposit for each sample a 100 nm-thick TiN bottom electrode (BE).

(Hf, Zr)O_2 thin films of 10 nm thickness were deposited onto previously fabricated TiN thin films. Then, a 50 nm-thick TiN is deposited onto the Si/TiN/(Hf, Zr)O_2 samples. UV photolithography and lift-off are used to obtain 100 nm-thick Pt top contact pads for electrical measurements. Fabrication settings are described in detail for TiN and (Hf, Zr)O_2 in Table I.

Characterizations are performed on as-deposited or annealed samples. Postmetallization annealing is realized under the conditions described in Table I.

B. Characterization

A 4-circles Smartlab Rigaku diffractometer with a high brilliance copper rotating anode is used for x-ray diffraction (XRD) in parallel beam configuration. As no monochromator is installed, a nickel filter is inserted to suppress the CuKα2 radiation.

X-ray photoelectron spectrometry (XPS) is achieved using the in-house XPS setup equipped with a standard AlKα monochromatic source at 1486.7 eV.

All electrical measurements were done on 50 μm diameter top pads. The electrical characterizations were systematically achieved in the same way: we first performed C–V characterization (using an HP-4284A LCR meter at 100 kHz in parallel mode). The leakage is then measured using an Agilent 4156B semiconductor parameter analyzer. Finally, positive up negative down (PUND) measurements are performed with a homemade setup. Triangular pulse rising time is 100 μs [an equivalent with dynamic hysteresis measurement (DHM) corresponds to 2.5 kHZ] at an amplitude high enough to saturate the P–E cycles: 3.8 V for sample annealed at 600 °C and 4 V for the other samples.

III. RESULTS AND DISCUSSION

Stoichiometry is measured by XPS on as-deposited 10 nm-thick (Hf, Zr)O_2 solid solutions without the top electrode. The present study examines two solid solutions, one grown at 5×10^{-3} mbar and one at 5×10^{-2} mbar. The stoichiometry is presented in Tables II and III.

The films are oxygen-deficient. On the one hand, during fabrication, the oxygen deficiency could favor the formation

TABLE II. Low pressure (LP): 5×10^{-3} mbar.

Elements	Stoichiometry	Error
Hf	0.54	± 0.03
Zr	0.46	± 0.03
O	1.8	± 0.1

TABLE III. High pressure (HP): 5×10^{-2} mbar.

Elements	Stoichiometry	Error
Hf	0.57	± 0.03
Zr	0.43	± 0.03
O	1.7	± 0.1

of the f-phase.[60,61] On the other hand, during cycling, it has also been demonstrated that fatigued stage is characterized by an increase of oxygen vacancies[25] linked to breakdown.

Then, the crystalline structure is analyzed as a function of the working pressure by grazing incidence x-ray diffraction (GIXRD). The reference patterns for TiN are from ICDD00-038-1420 and for (Hf, Zr)O_2 o-/t- and m-phases, reference patterns are, respectively, from Lee *et al.*[54] and ICDD04-002-5428. The two series of samples were annealed at 400, 500, and 600 °C.

Figure 1 shows GIXRD for LP and HP samples. The positions of the most intense peaks of the m- and o-/t-phases at theoretical values are represented. On LP [Fig. 1(a)], the m-phase is present even when the film is as-deposited, and the m-phase seems to be amplified when the temperatures increase. In particular, the peak at ≈ 34.5° becomes more and more visible, and the width of the peak m(11-1) decreases. On the contrary, the as-deposited HP [Fig. 1(b)] is amorphous. It remains amorphous when annealed at 400 °C. But, from 500 to 600 °C, an orthorhombic/tetragonal (o/t) peak appears at ≈ 30.7°. It is thought that the usual o/t peak is referenced between ≈ 30.5° (Ref. 54) and ≈ 30.8°.[62] In Fig. 1(b), this o/t peak is more intense than the remaining monoclinic one at ≈ 28.5°.

Consequently, having the amorphous phase for as-deposited (Hf, Zr)O_2 films seems to be crucial for the growth of the o/t-phase during the annealing step. It can be noticed that the sputtered HP (Hf, Zr)O_2 layer is still amorphous at 400 °C on the contrary to ALD-grown (Hf, Zr)O_2 layers.[8] We conclude that the crystallization takes place between 400 and 500 °C for HP samples.

ALD-grown (Hf, Zr)O_2 usually crystallizes at 400 °C after rapid thermal annealing (RTA). This difference can be attributed to the fact that ALD samples are deposited at around 250 °C [between 150 and 350 °C (Refs. 2, 7, 8, 11, and 20–42)], whereas in our process, depositions are done at room temperature.

He *et al.*[63] have also noticed in 2005 that the monoclinic phase seems to increase on sputtered undoped HfO_2 thin films

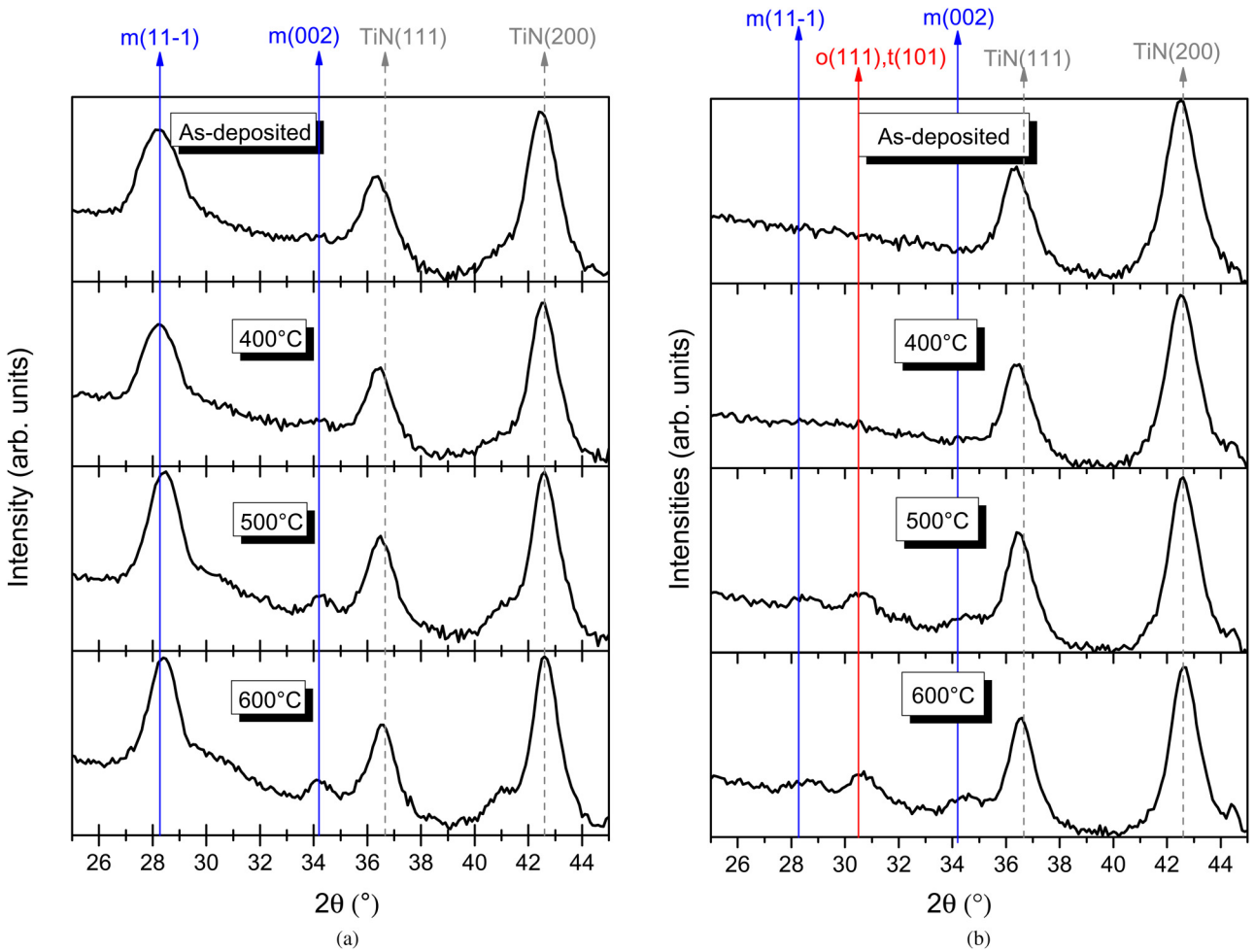

FIG. 1. GIXRD of (a) LP samples grown at 5×10^{-3} mbar: as-deposited and annealed at different temperatures. (b) HP samples: films grown at 5×10^{-2} mbar: as-deposited or annealed at different temperatures. Intensity is in log scale.

deposited on silicon. It would be possible that the increase of the monoclinic peaks with temperature is an intrinsic property of sputtered doped and undoped HfO_2 thin films.

Lee *et al.*[54] have showed that the monoclinic phase fraction increased with increase in the working pressure. The trend was opposite from the current work. However, fabrication details show the setup was very different from what is presented in this article: for instance, the target–substrate distances, the targets sizes, and the powers applied on the target are different. The TiN in the article of Lee *et al.* was deposited on an SiO_2/Si substrate, whereas it is deposited on Si(100) in our experiment, and TiN was deposited by direct current (DC) reactive sputtering instead of RF current reactive sputtering in our experiment.

Moreover, Lee *et al.* mention the fact that "the intensity of the diffraction peak from the *m*(111) planes increases as the working pressure increases." Such an increase could be attributed to a slight increase of the thickness since there is no electrical measurement to corroborate this statement.

To complete this study, electrical characterizations were conducted on 50 μm diameter circular pads. The measurements are shown only for HP because no ferroelectricity is expected nor observed for LP.

C–V measurements were performed to obtain the dielectric permittivity versus electrical field (Fig. 2). Samples annealed at 500 and 600 °C show the classic butterfly loop, which is typical of ferroelectric materials. Whereas the sample annealed at 400 °C does not exhibit such behavior. It is consistent with the GIXRD results: the butterfly loop is observed for samples showing the o/t-phase in GIXRD.

The relative permittivity ε_r range is found to be close to the values of standard ε_r generally observed for this ferroelectric material.[8]

P–E loop measurements (Fig. 3) were conducted to confirm ferroelectricity. Curves are corrected from leakage current by using the PUND techniques, and the data are shown here after 10^5 cycles. As expected, the samples annealed at 500 and 600 °C show open cycle characterizing ferroelectric behaviors, whereas the sample at 400 °C does not.

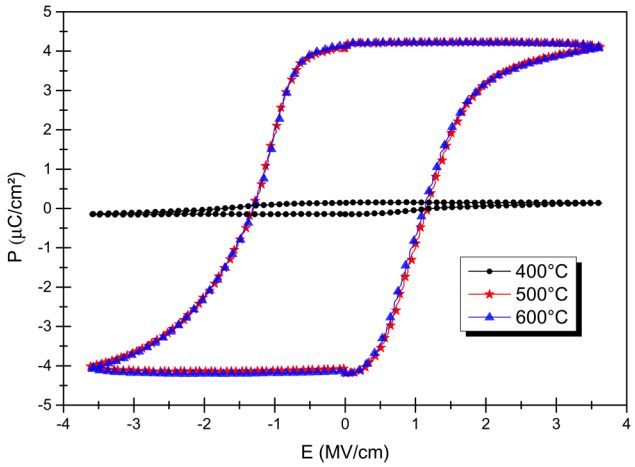

FIG. 3. P(E) hysteresis curves for TiN(100 nm)/(Hf, Zr)O_2(10 nm)/TiN(50 nm)/Pt(100 nm) annealed at 400, 500, and 600 °C after 10^5 PUND cycles.

Only the o-phase has been admitted as the crystalline phase giving rise to ferroelectricity. Consequently, the samples showing the orthorhombic peaks in GIXRD are ferroelectric.

The P_r values extracted from P–E loops for ferroelectric samples are around 5 μC/cm^2. It could seem quite low compared to the usual P_r values reported around 10−25 μC/cm^2.[64] However, this range of P_r values correspond to $Hf_{0.5}Zr_{0.5}O_2$ while our composition is $Hf_{0.57}Zr_{0.43}O_{1.7}$. Indeed, Park *et al.*[30] show that the P_r value is decreasing with the decrease of Zr concentration when Zr is between 0 and 0.5. Between 0.35 and 0.43, the P_r value seemed consistent with our results.

Moreover, our samples are not purely orthorhombic. P_r could be improved if the fraction of the monoclinic phase was decreased. Further works are in progress to identify the root cause of the low P_r.

Figure 4 shows the current density versus the electrical field. It can be seen that the leakage increases with the

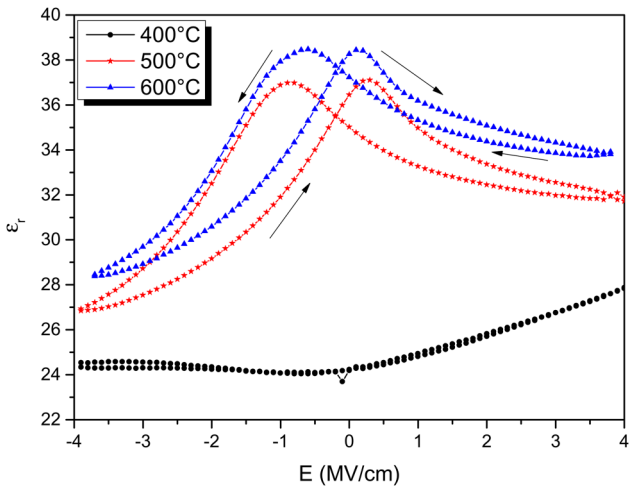

FIG. 2. Dielectric permittivity vs electrical field of TiN(100 nm)/(Hf, Zr)O_2(10 nm)/TiN(50 nm)/Pt(100 nm) samples as-deposited or annealed at 400, 500, and 600 °C.

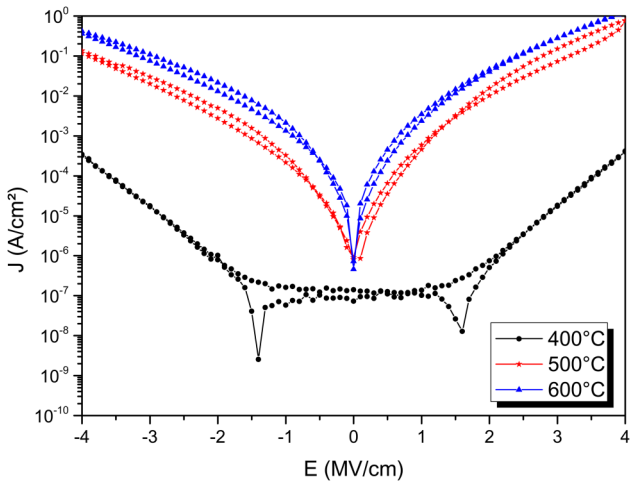

FIG. 4. Current density vs electrical field of TiN(100 nm)/(Hf, Zr)O_2(10 nm)/TiN(50 nm)/Pt(100 nm) annealed at 400, 500, and 600 °C before cycling.

annealing temperatures. The measurement seems to be close to what has been observed in cosputtering by Lee *et al.*[54]

IV. CONCLUSION

In this article, we have demonstrated that the deposition of ferroelectric (Hf, Zr)O_2 from a single hafnium/zirconium alloy target is effective and has advantages compared to ALD: The process is simpler since all depositions are made *in situ* in vacuum in the same chamber. It also reduces contamination issues. Moreover, depositions are extremely faster than ALD. However, further improvements have to be made, particularly in order to further increase the remnant polarization caused by a difficulty in controlling the stoichiometry of the (Hf, Zr)O_2 thin films.

Also, in 2015, Park *et al.*[64] wrote "So far, it seems critical that the dielectric layer is deposited in the amorphous phase and crystallized in a later annealing step." Here, by changing the working pressure, we report a clear evidence of this statement. In fact, (Hf, Zr)O_2 solid solutions were deposited by RF reactive magnetron sputtering at room temperature from a single Hf/Zr alloy target at two different pressures in the chamber. The growth of the m-phase has occurred at 5×10^{-3} mbar on the as-deposited sample, whereas at 5×10^{-2} mbar the film was amorphous. After an RTA, the monoclinic films stay in the m-phase, while the amorphous films crystallize in a mixture of the m- and o/t-phases. The temperature of the o/t-phase crystallization was between 400 and 500 °C. It has been clearly demonstrated that the films containing the o/t-phase were ferroelectric with a Pr of $5\,\mu C/cm^2$. Current work is in progress to increase P_r to the state of the art values.

ACKNOWLEDGMENTS

This work was realized on the NanoLyon technology platform and has received funding from the European Union's Horizon 2020 research and innovation programme under Grant Agreement No. 780302. The authors thank GDR OxyFun for its financial support. The authors also thank Ruben Vera (Centre de Diffractométrie Henri Longchambon, Université de Lyon) and Ingrid Cañero Infanto (Institut des Nanotechnologies de Lyon) for their help in the XRD data collection, Jérémy Stevens (Ecole Normale Supérieure de Lyon) for his help in the EDX data collection, Geneviève Grenet (Institut des Nanotechnologies de Lyon) and Claude Botella (Institut des Nanotechnologies de Lyon) for their help in the XPS data collection, and Aziz Benamrouche (Institut des Nanotechnologies de Lyon) for his help in the AFM data collection.

[1]S. Salahuddin and S. Datta, Nano Lett. **8**, 405 (2008), e-print arXiv:0707.2073.
[2]K.-S. Li *et al.*, "Sub-60 mV-swing negative-capacitance FinFET without hysteresis," in *2015 IEEE International Electron Devices Meeting (IEDM)* (IEEE, New York, 2015), pp. 22.6.1–22.6.4.
[3]J. F. Scott, *Ferroelectric Memories*, Springer Series in Advanced Microelectronics Vol. 3 (Springer, Berlin, 2000).
[4]Z. Fan, J. Chen, and J. Wang, J. Adv. Dielectrics **6**, 1630003 (2016).
[5]J.-M. Koo, "Fabrication of 3D trench PZT capacitors for 256Mbit FRAM device application," in *IEEE International Electron Devices Meeting 2005*, IEDM Technical Digest (IEEE, New York, 2005) pp. 340–343.
[6]C.-P. Yeh, M. Lisker, B. Kalkofen, and E. P. Burte, AIP Adv. **6**, 035128 (2016).
[7]T. S. Böscke, J. Müller, D. Bräuhaus, U. Schröder, and U. Böttger, Appl. Phys. Lett. **99**, 102903 (2011).
[8]M.-H. Park, H. Joon Kim, Y. Jin Kim, W. Lee, T. Moon, and C. Seong Hwang, Appl. Phys. Lett. **102**, 242905 (2013).
[9]X. Sang, E. D. Grimley, T. Schenk, U. Schroeder, and J. M. LeBeau, Appl. Phys. Lett. **106**, 162905 (2015).
[10]J. Müller *et al.*, J. Appl. Phys. **110**, 114113 (2011).
[11]J. Müller, T. S. Böscke, D. Bräuhaus, U. Schröder, U. Böttger, J. Sundqvist,P. Kücher, T. Mikolajick, and L. Frey, Appl. Phys. Lett. **99**, 112901 (2011).
[12]S. Mueller, J. Mueller, A. Singh, S. Riedel, J. Sundqvist, U. Schroeder, and T. Mikolajick, Adv. Funct. Mater. **22**, 2412 (2012).
[13]S. Mueller, C. Adelmann, A. Singh, S. Van Elshocht, U. Schroeder, and T. Mikolajick, ECS J. Solid State Sci. Technol. **1**, N123 (2012).
[14]T. Schenk, S. Mueller, U. Schroeder, R. Materlik, A. Kersch, and M. Popovici, "Strontium doped hafnium oxide thin films: Wide process window for ferroelectric memories," in *2013 Proceedings of the European Solid-State Device Research Conference (ESSDERC)*, Bucharest, Romania, 16–20 September 2013 (IEEE, 2013), pp. 260.
[15]A. G. Chernikova, D. S. Kuzmichev, D. V. Negrov, M. G. Kozodaev, S. N. Polyakov, and A. M. Markeev, Appl. Phys. Lett. **108**, 242905 (2016).
[16]Y. Sharma, D. Barrionuevo, R. Agarwal, S. P. Pavunny, and R. S. Katiyar, ECS Solid State Lett. **4**, N13 (2015).
[17]S. Starschich, D. Griesche, T. Schneller, and U. Böttger, ECS J. Solid State Sci. Technol. **4**, P419 (2015).
[18]S. Starschich and U. Boettger, J. Mater. Chem. C **5**, 333 (2017).
[19]L. Xu, T. Nishimura, S. Shibayama, T. Yajima, S. Migita, and A. Toriumi, Appl. Phys. Express **9**, 091501 (2016).
[20]A. J. Tan, A. K. Yadav, K. Chatterjee, D. Kwon, S. Kim, C. Hu, and S. Salahuddin, IEEE Electron Device Lett. **39**, 95 (2018).
[21]M. Kobayashi, N. Ueyama, K. Jang, and T. Hiramoto, IEEE J. Electron Devices Soc. **6**, 1 (2018).
[22]M. H. Park *et al.,* Nanoscale **9**, 9973 (2017).
[23]F. P. Fengler *et al.*, Adv. Electron. Mater. **3**, 1600505 (2017).
[24]S. J. Kim *et al.*, Appl. Phys. Lett. **111**, 242901 (2017).
[25]U. Schroeder *et al.*, "Impact of field cycling on HfO_2 based non-volatile memory devices," in *2016 46th European Solid-State Device Research Conference (ESSDERC)*, Lausanne, Switzerland, 12–15 September 2016 (IEEE, 2016), pp. 364–368.
[26]M. H. Park *et al.*, Nanoscale **10**, 716 (2018).
[27]T. Kim, J. Park, B.-H. Cheong, and S. Jeon, Appl. Phys. Lett. **112**, 092906 (2018).
[28]A. G. Chernikova, M. G. Kozodaev, D. V. Negrov, E. V. Korostylev, M. H. Park, U. Schroeder, C. S. Hwang, and A. M. Markeev, ACS Appl. Mater. Interfaces **10**, 2701 (2018).
[29]Y. Matveyev, D. Negrov, A. Chernikova, Y. Lebedinskii, R. Kirtaev, S. Zarubin, E. Suvorova, A. Gloskovskii, and A. Zenkevich, ACS Appl. Mater. Interfaces **9**, 43370 (2017).
[30]M. H. Park *et al.*, ACS Appl. Mater. Interfaces **8**, 15466 (2016).
[31]A. Chernikova *et al.*, ACS Appl. Mater. Interfaces **8**, 7232 (2016).
[32]S. L. Weeks, A. Pal, V. K. Narasimhan, K. A. Littau, and T. Chiang, ACS Appl. Mater. Interfaces **9**, 13440 (2017).
[33]S. W. Smith, A. R. Kitahara, M. A. Rodriguez, M. D. Henry, M. T. Brumbach, and J. F. Ihlefeld, Appl. Phys. Lett. **110**, 72901 (2017).
[34]A. Chouprik, A. Chernikova, A. Markeev, V. Mikheev, D. Negrov, M. Spiridonov, S. Zarubin, and A. Zenkevich, Microelectron. Eng. **178**, 250 (2017).
[35]G. Karbasian, R. Dos Reis, A. K. Yadav, A. J. Tan, C. Hu, and S. Salahuddin, Appl. Phys. Lett. **111**, 8 (2017).
[36]S. Zarubin, E. Suvorova, M. Spiridonov, D. Negrov, A. Chernikova, A. Markeev, and A. Zenkevich, Appl. Phys. Lett. **109**, 192903 (2016).
[37]S. Migita, H. Ota, H. Yamada, A. Sawa, and A. Toriumi, *2017 IEEE Electron Devices Technology and Manufacturing Conference (EDTM)*, Toyama, Japan, 28 February–2 March 2017 (IEEE, 2017), p. 255.
[38]S. Oh, T. Kim, M. Kwak, J. Song, J. Woo, S. Jeon, I. K. Yoo, and H. Hwang, IEEE Electron Device Lett. **38**, 732 (2017).
[39]P. D. Lomenzo, C. C. Chung, C. Zhou, J. L. Jones, and T. Nishida, Appl. Phys. Lett. **110**, 232904 (2017).

[40]J. Müller, T. S. Böscke, U. Schröder, S. Mueller, D. Bräuhaus, U. Böttger, L. Frey, and T. Mikolajick, Nano Lett. **12**, 4318 (2012).
[41]M. Hyuk Park, H. Joon Kim, Y. Jin Kim, T. Moon, and C. Seong Hwang, Appl. Phys. Lett. **104**, 72901 (2014).
[42]M. H. Park, H. Joon Kim, Y. Jin Kim, W. Lee, H. Kyeom Kim, and C. Seong Hwang, Appl. Phys. Lett. **102**, 112914 (2013).
[43]T. Shimizu, T. Yokouchi, T. Oikawa, T. Shiraishi, T. Kiguchi, A. Akama, T. J. Konno, A. Gruverman, and H. Funakubo, Appl. Phys. Lett. **106**, 112904 (2015).
[44]T. Shiraishi *et al.*, Appl. Phys. Lett. **108**, 262904 (2016).
[45]T. Shiraishi *et al.*, Mater. Sci. Semicond. Process. **70**, 239 (2017).
[46]T. Shimizu, T. Yokouchi, T. Shiraishi, T. Oikawa, P. S. S. R. Krishnan, and H. Funakubo, Jpn. J. Appl. Phys. **53**, 09PA04 (2014).
[47]K.-Y. Chen, P.-H. Chen, R.-W. Kao, Y.-X. Lin, and Y.-H. Wu, IEEE Electron Device Lett. **39**, 87 (2018).
[48]C. Abe, S. Nakayama, M. Shiokawa, H. Kawashima, K. Katayama, T. Shiraishi, T. Shimizu, H. Funakubo, and H. Uchida, Ceram. Int. **43**, S501 (2017).
[49]J. Y. Lee, G. Anoop, H. J. Lee, J. H. Kwak, and J. Y. Jo, Curr. Appl. Phys. **17**, 704 (2017).
[50]Y. Wei *et al.*, "A rhombohedral ferroelectric phase in epitaxially-strained $Hf_{0.5}Zr_{0.5}O_2$ thin films," Nat. Mater. **17**, 1095 (2018), e-print arXiv:1801.09008.
[51]F. Ambriz-Vargas, G. Kolhatkar, R. Thomas, R. Nouar, A. Sarkissian, C. Gomez-Yáñez, M. A. Gauthier, and A. Ruediger, Appl. Phys. Lett. **110**, 093106 (2017).
[52]S. Migita, H. Ota, H. Yamada, K. Shibuya, A. Sawa, and A. Toriumi, Jpn. J. Appl. Phys. **57**, 04FB01 (2018).
[53]K. C. Das, N. Tripathy, S. P. Ghosh, P. Sharma, R. Singhal, and J. P. Kar, Vacuum **143**, 288 (2017).
[54]Y. H. Lee, H. J. Kim, T. Moon, K. D. Kim, S. D. Hyun, H. W. Park, Y. B. Lee, M. H. Park, and C. S. Hwang, Nanotechnology **28**, 305703 (2017).
[55]F. Ambriz-Vargas *et al.*, ACS Appl. Mater. Interfaces **9**, 13262 (2017).
[56]F. Ambriz-Vargas, R. Thomas, and A. Ruediger, "Ferroelectric (Hf, Zr)O_2 thin films for high-density nonvolatile memories," in *Frontiers in Materials Processing, Applications, Research and Technology* (Springer, Singapore, 2018), p. 123.
[57]Z. Fan, J. Xiao, J. Wang, L. Zhang, J. Deng, Z. Liu, Z. Dong, J. Wang, and J. Chen, Appl. Phys. Lett. **108**, 232905 (2016).
[58]T. Kiguchi, S. Nakamura, A. Akama, T. Shiraishi, and T. J. Konno, J. Ceramic Soc. Jpn. **2**, 689 (2016).
[59]P. Polakowski and J. Müller, Appl. Phys. Lett. **106**, 232905 (2015).
[60]M. Hoffmann *et al.*, J. Appl. Phys. **118**, 072006 (2015).
[61]S. U. Sharath, J. Kurian, P. Komissinskiy, E. Hildebrandt, T. Bertaud, C. Walczyk, P. Calka, T. Schroeder, and L. Alff, Appl. Phys. Lett. **105**, 073505 (2014).
[62]E. Yurchuk, J. Müller, S. Knebel, J. Sundqvist, A. P. Graham, T. Melde, U. Schröder, and T. Mikolajick, Thin Solid Films **533**, 88 (2013).
[63]G. He, M. Liu, L. Zhu, M. Chang, Q. Fang, and L. Zhang, Surf. Sci. **576**, 67 (2005).
[64]M. H. Park *et al.*, Adv. Mater. **27**, 1811 (2015).